Research article

Automated vehicle driveaway with a manual dry clutch on chassis dynamometers: Efficient identification and decoupling control

Nikolaus Euler-Rolle [a],*, Christian H. Mayr [b], Igor Škrjanc [c], Stefan Jakubek [a], Gorazd Karer [c]

[a] Christian Doppler Laboratory for Innovative Control and Monitoring of Automotive Powertrain Systems, Institute of Mechanics and Mechatronics, TU Wien, Getreidemarkt 9/E325/A5, 1060 Vienna, Austria
[b] AVL List GmbH, Hans-List-Platz 1, 8020 Graz, Austria
[c] Faculty of Electrical Engineering, University of Ljubljana, Tržaška 25, 1000 Ljubljana, Slovenia

ARTICLE INFO

ABSTRACT

The testing and certification of vehicles in succession to their development are usually achieved on chassis dynamometer testbeds. In this context, the execution of test cycles shall be performed as automatised as possible even if vehicles with manual transmission powertrain are under test. A particular challenge is the vehicle driveaway from standstill by actuating clutch and engine in accordance with each other. In this paper a non-linear decoupling multivariate control scheme based on feedback linearisation considering the accelerator and clutch pedal positions as manipulated variables is proposed. To obtain the required vehicle model for control in a time-saving manner, the clutch torque transmissibility and engine torque characteristic are identified incorporating a Wiener model structure from efficiently designed drive manoeuvres. By applying this model structure, the dynamics can be considered separately from the static non-linearity, which is beneficial for control. In addition to the successful demonstration of the presented workflow and an examination of the controller performance on vehicle system simulation software, the robustness with respect to parameter uncertainties is investigated.

© 2019 ISA. Published by Elsevier Ltd. All rights reserved.

1. Introduction

When a newly developed vehicle is tested and certified in its entirety, usually chassis dynamometers are employed to assess the engine and powertrain performance referring to different aspects. Common criteria to be investigated are noise emission, performance, fuel consumption, exhaust emissions and electromagnetic compatibility. Compared to test runs on the road the use of testbeds is less expensive, easier to conduct, repeatable and can be fully automated, which is of importance in particular. In addition, chassis dynamometers allow for transient tests under pre-defined environmental conditions when they are located within a climate chamber. Also the easier integration of emission measurement devices, load control and data acquisition as compared to road tests is beneficial in a complete test cell system.

The automatisation of test runs is primarily enabled by a robotic device, which replaces and acts as a driver. Its tasks are the operation of the brake, the accelerator and the clutch pedal, as well as changing the gear by manipulating the gear lever. As usually a prescribed velocity profile and an associated gear shifting strategy have to be pursued, in terms of control engineering all

these actuators have to be considered as manipulated variables in a closed loop of the vehicle and a driver controller. Such a driver controller has to handle different tasks and is therefore composed of several overlying controllers treating driveaway, acceleration, gear shifts, deceleration and stopping.

In this paper, the non-linear multivariable decoupling control using the accelerator and clutch pedal for vehicle driveaway is considered for manual transmission powertrains as the first part of a holistic workflow for an automated testbed operation. The control scheme is based on feedback linearisation of multivariable systems [1] and incorporates a non-linear vehicle model. As soon as the clutch closes, one degree of freedom is lost and a different control strategy has to be applied. Also in this context, the application of feedback linearising control is advantageous and has been already applied for velocity control on chassis dynamometers with robotic drivers [2]. Hence, the velocity trajectory of an arbitrary test cycle can be tracked with high accuracy, although the control strategy has to be switched over during driveaway followed by the short distance driven in the first gear, as well as during shifting. The controller design in [2] does not require any a-priori information about the vehicle. In the context of multivariable decoupling control, such an assumption is too restrictive as at least the clutch characteristic varies too much in different vehicles and has to be identified in advance.

Especially the task of how to launch the vehicle from standstill on the testbed automatically is covered by the contribution in the present paper. The focus is on the provision of an efficient workflow to identify a vehicle and concurrently obtain a readily parameterised controller.

Thus, as the second main contribution of the present paper an identification procedure is proposed to be able to apply the controller to a previously unknown vehicle coming to the testbed without spending too much time for identification. This approach covers the identification of the dynamic engine torque characteristic in dependency of the accelerator pedal position as well as the clutch torque transmissibility characteristic. By applying a Wiener model structure [3], linear dynamics can be considered in feedback linearisation separately from the static non-linearity, which is beneficial for control.

The presented decoupling control scheme considers vehicle speed and engine speed as controlled variables. The accelerator pedal position and the clutch pedal position are the manipulated variables, which are actuated in accordance with each other. Compared to individual controllers, by application of a decoupling approach the controlled variables can track their reference trajectories without interacting with each other, which is the main benefit. As the considered non-linear vehicle and powertrain model has full relative degree when the required torques are considered as inputs, the decoupling control utilises these torques as intermediate manipulated variables. The inverse of the static non-linear transformation from the pedal positions to the required torques is considered after the controller separately. However, the dynamic behaviour of the torque buildup is included into the control scheme directly. This approach guarantees that the control scheme can be used with different model structures generically depending on the identified characteristic. Such models could for example also be neural networks resulting from deep learning.

Also, the robustness with respect to deviations of parameters such as for example the inertias or parameters of the torque buildup characteristic is demonstrated alongside a simulation with a modified clutch characteristic. For that purpose, parameter deviations are represented as a perturbation input to the error dynamics of the feedback linearised system. Finally, a lemma from non-linear control theory is applied showing the boundedness of errors.

Clutch control has been considered in the literature in various contexts. In [4] the relations from pedal positions to the torques are assumed to be linear and an analytic design procedure is applied to the overall linear model in the complex plane considering parameter variations, robust tracking and stability properties. A simple linear decoupling control for clutch engagement has also been shown by [5]. However, the control scheme is based on a simple linear second order model of the powertrain using torques as manipulated variables directly. When a controller replacing the driver is considered, only the pedal positions are available as manipulated variables. Thus, our workflow considers these variables in control directly. Several extensions of the linear control scheme of [5] put an emphasis especially on vehicle launch comfort, such as for example [6], who applied optimal control under consideration of the rate of change of the clutch torque as input instead of the clutch torque directly. In [7] the engagement of an automotive dry clutch using different mathematical formulations of the considered linear model is described and the proposed linear control scheme is further optimised. Based on these model formulations, other control methodologies have been demonstrated in the summarising book [8].

Also, the task of dual clutch control as it is required for gear shifting in automatic transmissions has been investigated in the literature. These control schemes usually combine different linear and non-linear controllers with a state machine to achieve reasonable gear shifting in diverse situations (e. g. [9–14]). In this context a feedback linearisation based feedforward–feedback control scheme has been applied to automatic dual clutch transmissions by [15]. This application to dual clutches focusing on shifting operation in production vehicles is not directly comparable to the start up controller considered for efficient testbed testing in this paper. However, a similar model structure and a non-linear engine torque characteristic are used.

When other non-linear properties of the powertrain are to be included into the model for control, often merely linear dynamic approximations or static non-linearities are used. In [16] the hydraulic clutch actuator position feedback loop is approximated by a first-order linear system and a static non-linear relation between clutch torque and clutch main bearing position is incorporated. Gear shifting control is then achieved based on cascaded and decoupled speed and torque control loops.

To consider the actual implementation of a clutch controller in a vehicle, additional attention has to be turned to parameter identification. In [17] parameters of a truck driveline model are identified using signals that are readily available on the vehicle data bus. Similar to the approach pursued in the present paper, the parameterisation is done by experiments with engaged clutch and steps on the accelerator pedal as excitation. However, only the inertias, stiffnesses and damping coefficients of the powertrain are estimated and the clutch torque is used as manipulated variable in two different optimal control strategies directly. In [18] an approach to also characterise the relation between the clutch main bearing position and the transmitted clutch torque is presented.

To summarise, the main contributions of this paper are the proposition of a holistic workflow to obtain a non-linear vehicle model for automated vehicle driveaway control as well as a non-linear decoupling multivariate control scheme based on feedback linearisation. Additionally, the robustness of the presented control scheme has been investigated. Overall, an advantageous and simple procedure is obtained to run vehicles with manual transmission powertrains in automated test runs on chassis dynamometer testbeds.

This paper is organised as follows: In Section 2 the powertrain model of a passenger vehicle is described, followed by the identification of its relevant parameters and characteristics in Section 3. The basic concept as well as the application of decoupling control to the vehicle launch are shown in Section 4. In Section 4.3 the controller robustness against parameter deviations is assessed. Finally, results for a passenger vehicle are given in Section 5.

2. Powertrain subsystems and models

Modelling and control of automotive powertrain systems is a broad field with a large amount of literature surveys [19–25] introducing the fundamentals of treating such systems. In the sequel, relevant subsystems of the powertrain (Fig. 1) and their basic equations as well as the overall model used in control are presented.

2.1. Engine model

Modern internal combustion engines are sophisticated mechatronic systems. Depending on the considered task, dynamic engine models with different fields of attention exist [25]. These models range from combustion fundamentals and in-cylinder processes with a resolution in the order of crank angle degrees (i. e. covered frequencies of 5–15 kHz) to mean value engine models, which consider the average dynamics over larger time intervals ranging from one combustion cycle up to a whole driving cycle of several minutes [26]. When control tasks from a driver's
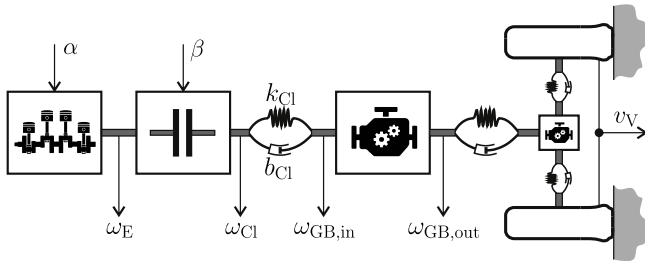
Fig. 1. Common manual transmission powertrain layout incorporating an internal combustion engine, dry clutch, gearbox, wheels and elastic shafts.

perspective are considered, especially the latter class of mean value engine models covering frequencies of about 0.1–50 Hz is suitable. The main dynamics of interest are those of the engine torque buildup as response to the accelerator pedal position α, which usually shows a highly non-linear dynamic behaviour. The equation of motion of the engine is

$$J_E \dot{\omega}_E = T_E(\alpha, \omega_E, \cdot) - T_{Cl}(\cdot) \tag{1}$$

with engine inertia J_E, the engine torque T_E and the torque T_{Cl} transmitted by the clutch. The torques can be modelled as functions depending on several quantities, which is indicated by a dot in the argument.

Although there exist non-linear engine models with only a few number of states [27], their application in launch control is not suitable. The model states such as turbocharger speed, subsystem actuator positions or manifold pressures are neither known to a driver, nor available in production vehicles. Hence, a reasonable tradeoff between model complexity and necessary parameterisation effort is required. The applied Wiener model structure, which is comparable to [28], for representation of T_E is easy to parameterise, yet sufficiently accurate.

2.2. Clutch model

In vehicles with manual transmissions usually a single plate friction clutch is used transmitting power by means of friction. Additionally, an automotive dry clutch disc is equipped with torsional dampers resulting in a piece-wise linear surrogate torsional stiffness behaviour. The equation of motion of the clutch in sliding state is

$$J_{Cl,out} \dot{\omega}_{Cl} = T_{Cl}(\cdot) - T_S - b_{Cl}(\omega_{Cl} - \omega_{Gb,in}), \tag{2}$$

where $J_{Cl,out}$ is the inertia of the clutch output part attached to the transmission, ω_{Cl} is the clutch disk rotational speed, $\omega_{Gb,in}$ is the rotational speed of the gearbox input shaft and b_{Cl} is a damping coefficient. The surrogate elasticity of the clutch is described by torque T_S as

$$\dot{T}_S = k_{Cl}(\varphi_{Cl})(\omega_{Cl} - \omega_{Gb,in}), \tag{3}$$

which is governed by the non-linear stiffness characteristic $k_{Cl}(\varphi_{Cl})$ depending on the relative angular displacement φ_{Cl} between the clutch disk and the gearbox input shaft.

The most essential part of the clutch model is the relation between the clutch torque T_{Cl} and the pedal position β, or the clutch main bearing position x_{MB}, respectively. A common representation of T_{Cl} is the result of a Coulombic friction model

$$T_{Cl} = F_n \mu R_{Cl} \, \text{sign}(\omega_E - \omega_{Cl}) \tag{4}$$

with normal force F_n acting between the two clutch disks, the (dynamic) friction coefficient μ and a characteristic clutch disk

radius R_{Cl}. The slip speed $\omega_{sl} = \omega_E - \omega_{Cl}$ determines the direction of the torque transmission, but not its magnitude in this static model. Eq. (4) defining the torque transmissibility is widely used in the literature, for example by [7,29] or [8]. Extensions have been made by modelling μ dependent of slip speed and temperature [30], by considering the clutch disk radius R_{Cl} as variable during the engagement [31], by modelling the non-linear relation between the normal force F_n and the normalised clutch pedal position β via the cushion spring characteristic [8] or by adding the hydraulic system to the torque transmissibility model [32]. As soon as the clutch disc friction facings wear out, the torque transmissibility characteristic changes usually by experiencing a shift without changing its shape significantly [29,33].

When control tasks are considered, only lumped clutch models, which confine themselves to describe the transmitted torque phenomenologically, should be used. In the identification in Section 3, such a lumped model is used, which comprises a static non-linearity in combination with first order linear dynamics.

2.3. Gearbox and differential

Usually, the stiffness encountered in the gearbox is much larger compared to other components of the remaining powertrain. Thus, for launch control the gearbox is modelled as a rigid device without any dynamic behaviour. Additionally, when considering the driveaway, also the backlash can be neglected. Depending on the selected gear i the transmission ratio

$$r_{G,i} = \frac{\omega_{in}}{\omega_{out,i}} = \frac{T_{out,i}}{T_{in}} \tag{5}$$

changes. For automotive transmissions, $r_{G,i} > 1$ holds for the lower gears, whereas higher gears might be realised with a transmission ratio of less than one. For $r_{G,i} > 1$ the rotational speed is reduced from ω_{in} to $\omega_{out,i}$ at the output and the torque $T_{out,i}$ is increased from T_{in}, respectively. The equation of motion of the gearbox is

$$J_{Gb,out} \dot{\omega}_{Gb,out} = r_{G,i} \left(T_S + b_{Cl}(\omega_{Cl} - \omega_{Gb,in}) \right) - T_{Gb,out}, \tag{6}$$

where $J_{Gb,out}$ is the inertia of the gearbox reduced to the output shaft and $T_{Gb,out}$ is the torque at the output shaft. To obtain the overall transmission ratio r_i of the powertrain from the engine rotational speed to that of the wheels in gear i, also the differentials and the final drive have to be included. The overall transmission ratio r_i is the product of the transmission ratio of the gearbox and that of all differentials r_D

$$r_i = r_D r_{G,i}. \tag{7}$$

2.4. Shafts

Depending on the powertrain layout adjacent components such as the gearbox, differentials and wheels are connected by elastic shafts. These elastic connections, especially the half shafts attached to the wheels, would have to be included according to the specific layout of the considered powertrain (e. g. Fig. 1). However, when the powertrain is controlled by the pedal positions, higher frequency oscillations cannot be considered in control. Thus, elastic connections are insignificant in the current control task and are assumed stiff.

2.5. Wheels and longitudinal dynamics

Especially when powertrain oscillations and the corresponding longitudinal vehicle dynamics are to be analysed, an accurate tyre model represents an essential part of the overall model. However, tyre dynamics are a difficult to model and highly non-linear
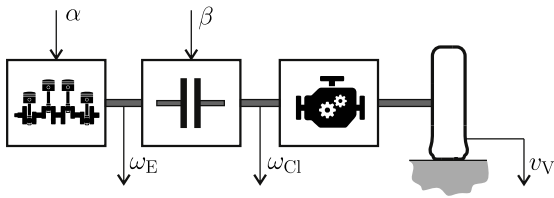
Fig. 2. Powertrain model applied in decoupling control.

process [34]. To control the vehicle from a driver's perspective (i. e. using the accelerator and clutch pedal only), such oscillations cannot be considered directly. It is already in the design and calibration of underlying control loops that powertrain oscillation reduction would have to be considered, for example by ensuring a suitable torque build up characteristic [25].

In the application to driveaway control, straight line driving is assumed such that the wheel speed of all wheels is equal. Also, the torques supplied by the differentials are distributed equally to both wheels and both axes, respectively. Then, the vehicle can be reduced to a single mass m_V, whose longitudinal movement is directly related to the angular velocity of the wheels by the dynamic rolling radius R_W of the wheels

$$\left(J_W + m_V R_W^2 \right) \dot{\omega}_W = T_W - R_W F_{Res}(v_V). \tag{8}$$

The overall wheel torque T_W accelerates the vehicle, whereas the driving resistance F_{Res}, which is usually a function of vehicle velocity v_V, opposes the acceleration. If more elaborate tyre models are used, non-linear relations exist between the longitudinal vehicle velocity, the wheel speed and the effective longitudinal force.

2.6. Model for decoupling control

Combining the dynamic relations of all submodels (1), (2), (3), (4), (6), (8) and their elastic connections yields a detailed non-linear dynamic model describing the powertrain and the longitudinal vehicle dynamics, respectively. The model complexity and the large amount of involved parameters, which are difficult to obtain in general, are disadvantageous for the application in control tasks considering a driver's perspective.

To obtain a reduced complexity model (Fig. 2) adequate for control, elastic connections are assumed rigid. The vehicle model with slipping clutch basically reduces to the equation of motion of the engine (1) and that of the remaining powertrain

$$J'_{V,i} \dot{\omega}_{Cl} = T_{Cl}(\cdot) - T'_{R,i}(v_V) \tag{9}$$

where $J'_{V,i}$ denotes the reduced (indicated by $'$) moment of inertia of the powertrain from the clutch output side to the vehicle mass in gear i. In the most simplifying assumption $J'_{V,i}$ could be reduced to the combination of the moment of inertia J_W of the wheels and the influence of vehicle mass m_V

$$J'_{V,i} = \frac{1}{r_i^2} J_{V,i} \approx \frac{1}{r_i^2} \left(J_W + m_V R_W^2 \right). \tag{10}$$

The torque $T'_{R,i}(v_V)$ results from driving resistance. The identification of its approximation from coast down acceleration data will be described in Section 3.1.

Finally, as manipulated variables only the pedal positions α and β are available. Thus, two additional model equations describing the dynamic torque characteristics of the engine torque T_E as well as the clutch torque T_{Cl} have to be used. In their most general form, these are represented by non-linear dynamic models

$$t_E \left(T_E^{(n_E)}, \ldots, \dot{T}_E, T_E, \alpha^{(n_E)}, \ldots, \right.$$

$$\left. \dot{\alpha}, \alpha, \omega_E^{(n_E)}, \ldots, \dot{\omega}_E, \omega_E, \cdot \right) = 0 \tag{11a}$$

$$t_{Cl} \left(T_{Cl}^{(n_{Cl})}, \ldots, \dot{T}_{Cl}, T_{Cl}, \beta^{(n_{Cl})}, \ldots, \right.$$

$$\left. \dot{\beta}, \beta, \omega_{sl}^{(n_{Cl})}, \ldots, \dot{\omega}_{sl}, \omega_{sl}, \cdot \right) = 0 \tag{11b}$$

depending on several variables. The identification and determination of the structure of (11) as well as of the driving resistance will be shown in Section 3.

3. Identification

It is obvious that the model parameters vary among different vehicle-types. Furthermore, auxiliary forces and torques caused by, e.g., various road-gradients also significantly influence the dynamic properties of a vehicle. However, as the model of vehicle dynamics is primarily intended for control purposes, the most general structure of the model (11) is not adequate. A control approach based on a too complex model could become intractable. In addition, such a model would require estimating a large number of interconnected parameters from a limited set of the available – often noisy – measurements. Hence, a useable structure of the model should be revealed by carrying out well-designed experiments.

- The experiments must be designed so that they can be carried out in a real vehicle testing environment.
- The measurements should be automatised and conducted in as limited time as possible; when human intervention is unavoidable, it should be kept to the minimum extent.
- The measured variables and signals should be available directly or indirectly from the real vehicle.
- No direct torque measurements are available.
- The measurements should be processed in an algorithmized manner.
- The results should be formatted so that the resulting model can directly be implemented in the control approach.
- The experiment design should reflect the way humans learn to drive, i.e., to operate the accelerator pedal position α and the clutch pedal position β.

The simulation experiments were conducted within *CarMaker® pro* and *AVL CRUISE™ M*, which are advanced dedicated software environments produced by IPG Automotive and AVL, respectively. The simulation solutions are developed specifically for testing passenger cars and light-duty vehicles. Using the software, it is possible to accurately model real-world test scenarios, including the entire surrounding environment. *CarMaker® pro* and *AVL CRUISE™ M* are open integration and test platforms and can be applied throughout the entire development process – from model – to software – to hardware – to vehicle-in-the-loop.

The simulated experiments can be used to master the current requirements of vehicle development. In accordance with the automotive systems engineering approach, the virtual test driving is used to develop and test systems and system networks in their entirety within the whole vehicle in realistic scenarios. The simulation solution includes a complete model environment comprising a detailed vehicle model and highly flexible models for roads and traffic. With the aid of this model environment, it is possible to build complete and realistic test scenarios, taking the test run off the road and conducting it using computer simulation. The event and manoeuvre-based testing method ensures that the necessary flexibility and realistic execution of real-world test driving are also features of virtual test driving. Various examples of successful simulated virtual-drive approach implementations have been extensively documented in literature [35–42].
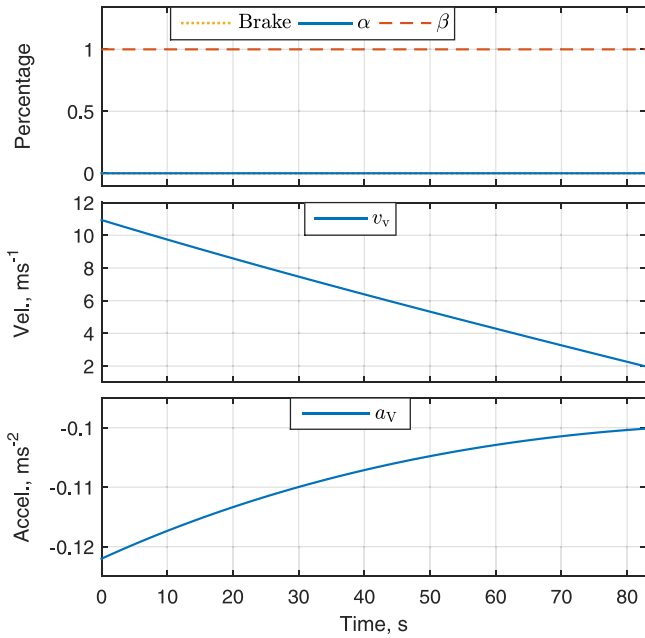
Fig. 3. Section of the simulation experiment conducted for the driving-resistance identification; Upper panel: accelerator (blue solid line), clutch (red dashed line) and brake pedal position (dotted line); Middle panel: vehicle speed (blue solid line); Lower panel: vehicle acceleration (blue solid line).
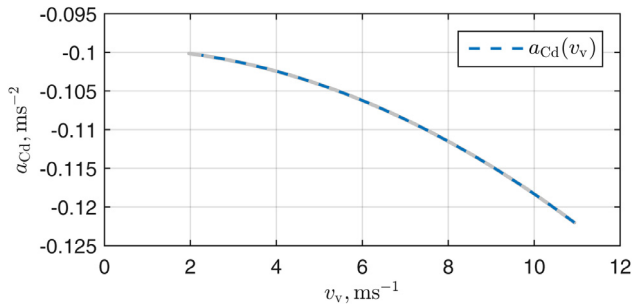

Fig. 4. Processed data (grey dots) and fitted polynomials (blue dashed line) of coast-down acceleration a_{Cd} with regard to vehicle speed v_V.

The simulations were carried out using a typical passenger front-wheel driven car model. As the simulation models are of high fidelity, we do not expect any considerable deviations of the dynamic behaviour as compared to the usage of actual data instead of simulations, provided the parameters are validated and measurement noise is not dominant. Therefore, we believe that the conducted simulations adequately represent real testbed experiments. However, real testbed experiments will have to be carried out in the future in order to prove the applicability of the presented approach in practice.

The identification section consists of 4 subsections.

First, the driving resistance is treated. The identification is carried out using coast-down experiment data, which provides enough information to identify the effective resistance torque measured as coast-down acceleration.

Next, the engine torque is considered. A Wiener nonlinear model structure is assumed. As the achievable engine torque depends on the accelerator pedal position as well as the actual engine speed, the engine-torque map identification must be carried out considering both influential variables. The identification data is obtained from adequately designed experiments so that the whole relevant operating range is taken into account.

Furthermore, clutch torque transmissibility is identified from several driveaway experiments with different clutch positions. During the experiments, the engine speed is kept constant using a simple feedback controller.

Finally, an inverted engine characteristic is derived. The resulting characteristic is a bijective mapping that is used in the proposed decoupling control scheme.

3.1. Driving resistance

The reduced driving resistance torque $T'_{R,i}(v_V)$ acting at the clutch appears in (9). It depends on the selected gear and incorporates all effects, which increase the required power to maintain a demanded vehicle velocity, and includes e. g. the friction of powertrain components, air resistance, road gradient and various other sources of power losses. Usually, the driving resistance is described in form of a quadratic polynomial depending on the vehicle velocity v_V. By performing a coast down experiment or simulation, where the vehicle is accelerated to a certain velocity and rolls to a stop with clutch open, this polynomial can be parameterised easily. In the application to the decoupling control, instead of the torque the magnitude of acceleration

$$a_{Cd}(v_V) = \text{sign}(v_V)\left(a_0 + a_1|v_V| + a_2 v_V^2\right) \tag{12}$$

is modelled directly as it is easier measurable and can be beneficially applied in the subsequent equations for vehicle identification. The relation of $a_{Cd}(v_V)$ and $T'_{R,i}(v_V)$ will be derived in the next section.

Usually, the polynomial coefficients a_0, a_1 and a_2 are determined as the first identification task. Frequently these coefficients are already available for certain vehicles, because they are a necessary information for the chassis dynamometer testbed controller. The coast-down simulation experiment is shown in Fig. 3. The parameters in Eq. (12) can be identified from the experimental data. For the particular car, the identified driving-resistance characteristic is shown in Fig. 4. The coast-down parameters are as follows.

$$a_0 = -9.94 \cdot 10^{-2} \text{ m s}^{-2}$$
$$a_1 = -1.62 \cdot 10^{-8} \text{ s}^{-1} \tag{13}$$
$$a_2 = -1.89 \cdot 10^{-4} \text{ m}^{-1}$$

Due to the structure of $a_{Cd}(v_V)$, a discontinuity occurs at velocity zero, which is especially disadvantageous in startup control. As a simple yet effective solution the sign function in (12) can be approximated by a tanh function to remove the discontinuity [43].

3.2. Engine torque

Besides depending on the accelerator pedal position α, the achievable engine torque T_E varies according to the actual engine speed ω_E as well. The map identification must therefore be conducted considering both influential variables $T_E(t) = T_E(\alpha(t), \omega_E(t))$. During normal vehicle operation the actual engine speed ω_E is subject to constant variations, thus it is generally not possible to carry out steady-state torque measurements: the accelerator pedal position α can easily be fixed to a certain value, but the steady state can generally not be reached, especially for higher values of α (in 1st gear and on flat road) as the resulting engine torque quickly accelerates the engine speed ω_E beyond its maximum limit, which results in the underlying engine controller taking over rendering such measurements useless. Therefore, the engine torque map must be identified using dynamic experiments by measuring the vehicle velocity and acceleration that are (indirectly) influenced by the actual engine torque T_E with regard to the accelerator pedal position α and the actual engine speed
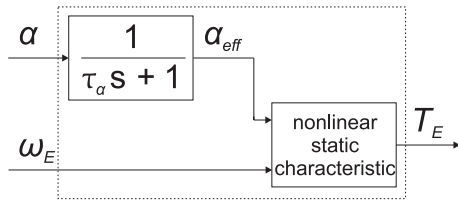
Fig. 5. Block diagram of the Wiener model describing the engine torque characteristic.
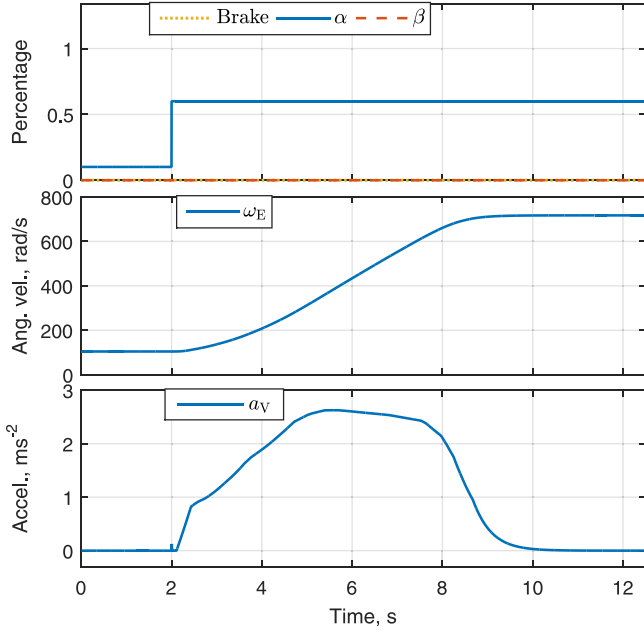

Fig. 6. Section of the simulation experiment conducted for the engine torque identification; Upper panel: accelerator (blue solid line), clutch (red dashed line) and brake pedal position (dotted line); Middle panel: engine speed (blue solid line); Lower panel: vehicle acceleration (blue solid line).

ω_{E}. As explained in Section 2.1, the engine torque characteristic $T_{\mathrm{E}} = T_{\mathrm{E}}(\alpha, \omega_{\mathrm{E}})$ is modelled as a Wiener model. A block diagram of the Wiener model is depicted in Fig. 5. A simple 1st order dynamics for the accelerator pedal position α is assumed

$$\dot{\alpha}_{\mathrm{eff}}(t) = \frac{\alpha(t) - \alpha_{\mathrm{eff}}(t)}{\tau_{\alpha}}, \qquad (14)$$

where τ_{α} denotes the time constant that describes the dynamic part of the Wiener model. The effective accelerator pedal position α_{eff} represents the input of the static part of the Wiener model $T_{\mathrm{E}}(t) = T_{\mathrm{E,stat}}(\alpha_{\mathrm{eff}}(t), \omega_{\mathrm{E}}(t))$.

It is clear that such a model is generally too coarse to fully approximate the dynamics of the torque build-up, but the primary aim is to develop a model that is adequate for control purposes, thus the simple structure is sufficient. Furthermore, the simplicity makes it easy to identify the model parameters using relatively simple experiments that can be conducted in a real-world setting without requiring too much effort nor taking a long time to carry out. In addition, such an approach is also suitable for vehicles that allow different driving modes (sport, comfort), where the accelerator pedal position α is appropriately filtered in order to obtain the value that represents the actual input of the engine. Hence, the dynamics in Eq. (14) allow a simple approximation of various engines and vehicles. The simulation experiments are conducted by feeding various step signals representing the accelerator pedal position α as the input. The appropriate response

trajectories of the engine and the vehicle are recorded. Note that the identification simulations are conducted with the clutch fully engaged ($\beta = 0$). An exemplary section of the identification data is shown in Fig. 6. The identification data is compiled from several measurements for various positions of accelerator pedal position α, accelerating from various initial engine speeds: the simulation experiments involved accelerations invoked by setting the accelerator pedal positions to $\alpha \in \{0.1, 0.2, \ldots, 1.0\}$, starting from initial engine speeds $\omega_{\mathrm{E}}/\mathrm{RPM} \in \{1000, 1500, 2000\}$, respectively. The signals can be easily generated automatically or by an operator so that the whole operating range can be covered.

There is a trade-off between the accuracy of the identification results and the time needed to conduct the experiments in order to gather an adequate amount of identification data. However, a set of experiments consisting of several runs similar to the one shown in Fig. 6 can be carried out fairly quickly in practice. One experiment run takes less than 10 s. In order to cover the whole operating range, it is more than adequate to conduct 10×3 runs ($\alpha \in \{0.1, 0.2, \ldots, 1.0\}$; $\omega_{\mathrm{E}}/\mathrm{RPM} \in \{1000, 1500, 2000\}$). Hence, less than 5 min of experimentation data is needed, which is not difficult to achieve on a testbed. Despite the time needed for experiments being quite sensible, adequate measurements for satisfactory identification could be recorded by even further reducing the experimentation time, if so required.

By measuring the longitudinal acceleration of the vehicle and taking into account the dynamic relations, it is possible to identify and derive the torque map $T_{\mathrm{E}} = T_{\mathrm{E}}(\alpha_{\mathrm{eff}}, \omega_{\mathrm{E}})$ as follows. Considering Newton's second law for rotation

$$\dot{\omega}_{\mathrm{E}} \underbrace{\left(J_{\mathrm{E}} + J'_{\mathrm{V},i} \right)}_{J^*(r_i)} = T_{\mathrm{E}}(\alpha_{\mathrm{eff}}, \omega_{\mathrm{E}}) - T'_{\mathrm{R},i}(v_{\mathrm{V}}), \qquad (15)$$

where $J^*(r_i)$ denotes the moment of inertia of the whole vehicle and powertrain, and Newton's second law for longitudinal vehicle acceleration

$$a_{\mathrm{V}} = \frac{R_{\mathrm{W}}}{r_i} \dot{\omega}_{\mathrm{E}}, \qquad (16)$$

it is possible to express a_{V} with torques

$$a_{\mathrm{V}} = \frac{R_{\mathrm{W}}}{r_i J^*(r_i)} \left(T_{\mathrm{E}}(\alpha_{\mathrm{eff}}, \omega_{\mathrm{E}}) - T'_{\mathrm{R},i}(v_{\mathrm{V}}) \right). \qquad (17)$$

By substituting the driving resistance torque $T'_{\mathrm{R},i}(v_{\mathrm{V}})$ by coast down acceleration a_{Cd}, a_{V} can be reformulated as

$$a_{\mathrm{V}} = \frac{R_{\mathrm{W}}}{r_i J^*(r_i)} T_{\mathrm{E}}(\alpha_{\mathrm{eff}}, \omega_{\mathrm{E}}) - \frac{J'_{\mathrm{V},i}}{J^*(r_i)} \underbrace{\frac{R_{\mathrm{W}}}{r_i J'_{\mathrm{V},i}} T'_{\mathrm{R},i}(v_{\mathrm{V}})}_{-a_{\mathrm{Cd}}(v_{\mathrm{V}})}. \qquad (18)$$

Thus, the driving resistance torque $T'_{\mathrm{R},i}(v_{\mathrm{V}})$ can be expressed as

$$T'_{\mathrm{R},i}(v_{\mathrm{V}}) = -\frac{r_i J'_{\mathrm{V},i}}{R_{\mathrm{W}}} a_{\mathrm{Cd}}(v_{\mathrm{V}}). \qquad (19)$$

Considering that $J'_{\mathrm{V},i} \gg J_{\mathrm{E}}$, Eq. (18) can be rewritten as

$$\frac{T_{\mathrm{E}}}{J^*} \approx \frac{r_i}{R_{\mathrm{W}}} \left(a_{\mathrm{V}} - a_{\mathrm{Cd}}(v_{\mathrm{V}}) \right). \qquad (20)$$

In this manner, it is possible to identify and derive the engine torque map by measuring the longitudinal acceleration of the vehicle.

The dynamic part of the Wiener model (see Eq. (14)) is obtained using the Nelder–Mead optimisation method. For each data point, the effective accelerator pedal position α_{eff} is calculated from the signal $\alpha(t)$ with regard to the actual value of the time constant τ_{α} within the particular optimisation step. The resulting data is compared to the identified engine torque
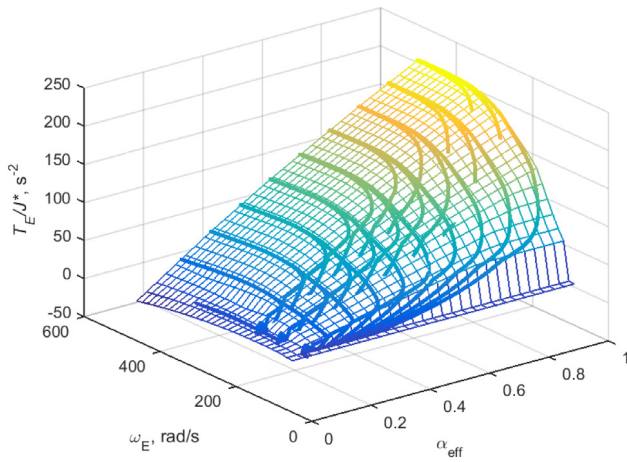
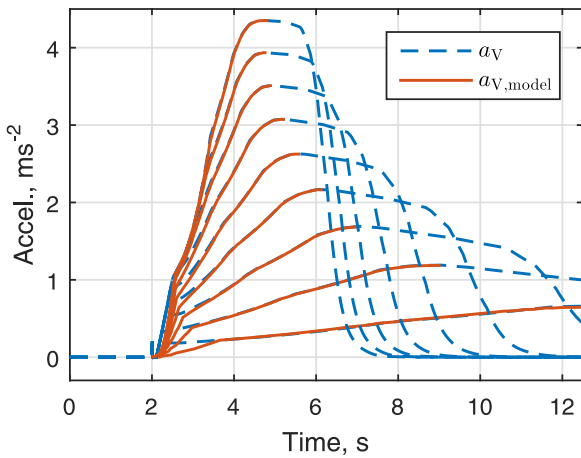**Fig. 7.** Engine torque map (wireframe mesh) and identification data.

Fig. 8. Series of simulated measured acceleration experiments a_V (blue dashed line) compared to the outputs of the identified model $a_{V,model}$ (red solid line).

map $\frac{T_E}{J^*} = \frac{T_E(\alpha_{eff}, \omega_E)}{J^*}$ and the average square error between the measured data $\{\frac{T_E}{J^*}\}_{measured}$ and the simulated data $\{\frac{T_E}{J^*}\}_{simulated}$ is used as the criterion f_{crit} for the optimisation:

$$f_{crit} = \frac{1}{N} \sum_{i=1}^{N} (\{\tfrac{T_E}{J^*}\}_{measured}(i) - \{\tfrac{T_E}{J^*}\}_{simulated}(i))^2 \qquad (21)$$

where $i \in \{1, \ldots, N\}$ is the index of measured or simulated data point. For the particular vehicle, the optimisation establishes the following time constant of the Wiener model

$$\tau_\alpha = 0.3546 \text{ s}. \qquad (22)$$

Fig. 7 depicts the resulting engine torque map. The actual torque depends on the effective accelerator pedal position α_{eff} and the engine speed ω_E. The depicted wireframe mesh represents the identified engine torque map, whereas the overlying trajectories show the identification data.

In order to verify the identified engine torque model we conduct a series of acceleration experiments that are most relevant for the vehicle driveaway problem. The experiments are carried out with various final accelerator pedal positions α so that the whole relevant operating range is taken into consideration. The simulated measured acceleration data a_V are compared to the outputs of the identified model $a_{V,model}$. The comparison is shown in Fig. 8.
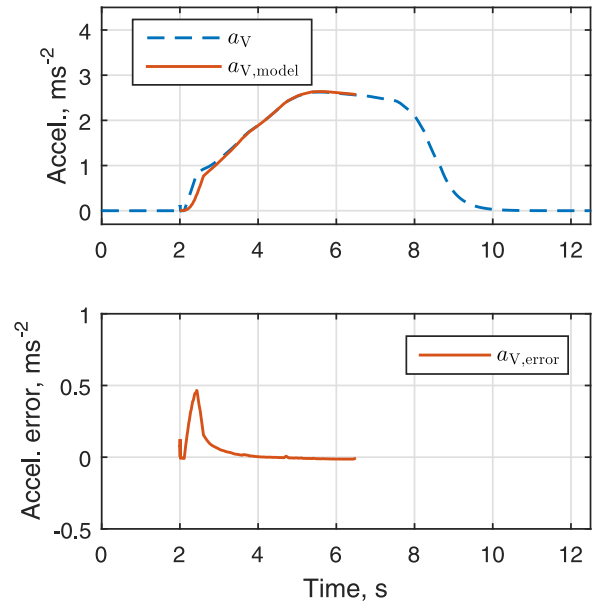

Fig. 9. Simulated measured acceleration signal a_V (blue dashed line) compared to the output of the identified model $a_{V,model}$ (red solid line). Below, the error signal $a_{V,error} = a_V - a_{V,model}$ within the relevant time-interval is shown (red solid line).

Furthermore, the results of the experiment (with similar inputs as in Fig. 6 – i.e., $\alpha_{fin} = 0.6$) are compared to the output of the identified model. The signals a_V and $a_{V,model}$ along with the resulting modelling error signal $a_{V,error} = a_V - a_{V,model}$ within the relevant time-interval are depicted in Fig. 9.

3.3. Clutch torque transmissibility

For the identification of the clutch torque transmissibility, simulation experiments are conducted with the clutch pedal. The resulting vehicle acceleration is recorded to determine the characteristic of torque transmission through the clutch. In the application to a vehicle on the testbed, a human driver could simply perform the experiments by executing several driveaways with different clutch positions. In simulation, the engine speed is kept at a constant value by a feedback controller, whereas the clutch and brake are operated open loop. Thus, these open loop signals have to be designed in an appropriate manner.

In Fig. 10 a section of the simulation experiment is depicted. The clutch is fully disengaged at $\beta = 1$ (red dashed line in the upper panel). Driveaways are performed by steps or steps in combination with ramp signals, and the resulting acceleration a_V (lower panel) is recorded. In between the experiments the vehicle is brought to a halt using the brake pedal (dotted line in the upper panel). In that way appropriate data for identification can be obtained in a short period of time with available measurement devices.

Motivated by physical considerations as well as by analysis of the obtained data, the torque transmissibility is basically considered as a static non-linearity depending on the clutch pedal position only. Thus, the obtained acceleration data are fitted by a third order polynomial. In Fig. 11 two different acceleration characteristics and the data for identification are depicted.

The required torque characteristic is found by rewriting (9) using (12) and the relation $a_V = R_W r_i^{-1} \dot{\omega}_{Cl}$

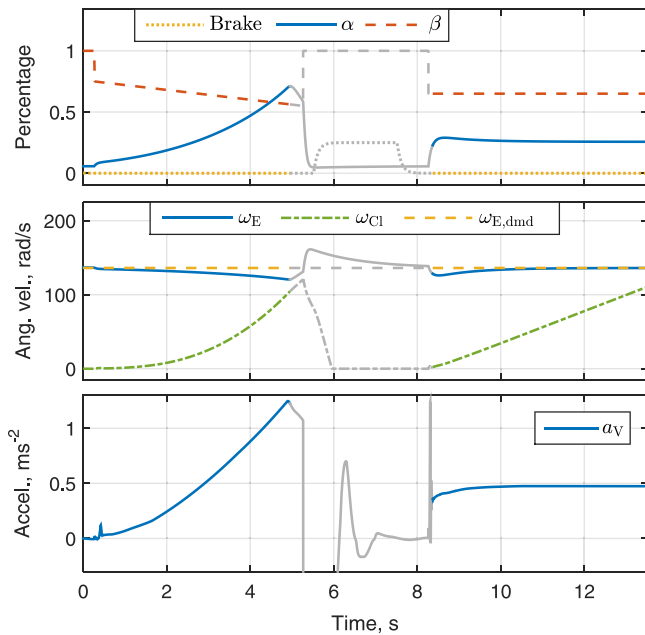$$\frac{T_{Cl}}{J'_{V,i}} = \frac{r_i}{R_W} (a_V + a_{Cd}). \qquad (23)$$

Fig. 10. Section of the simulation experiment conducted for the clutch torque transmissibility identification; Upper panel: accelerator (blue solid line), clutch (red dashed line) and brake pedal position (dotted line); Middle panel: engine speed (blue solid line), reference value (yellow dashed line) and clutch disc speed (green dash-dotted line); Lower panel: vehicle acceleration (blue solid line); Interval not considered in the identification is greyed out.
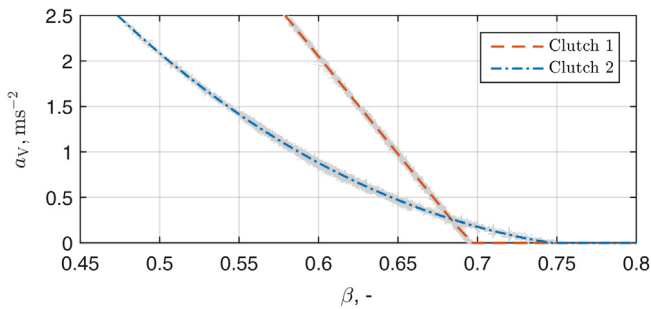

Fig. 11. Processed data (grey dots) and fitted polynomials (dashed and dot-dashed line) of recorded vehicle acceleration a_V for two different clutches.

As it is assumed that the engine always delivers a sufficient amount of engine torque, the recorded torque (23) can be considered as the maximum clutch torque.

To obtain an overall vehicle model suitable for decoupling control, the clutch characteristic is extended to a Wiener model using first order low pass dynamics with a fast time constant of 10 ms as compared to the rest of the system. Primarily, this extension is motivated by the mathematical structure of the vehicle powertrain model to significantly simplify the controller design and be able to include the clutch torque as a system state (see Section 4). Nevertheless, either the hydraulic system dynamics between clutch pedal and the clutch itself or the dynamics of the robotic device acting as a driver could be considered as an physical interpretation of the low pass behaviour.

3.4. Map inversion

In the final application of the control scheme, the decoupling controller will consider the dynamics of the engine and clutch torque buildup. Their static non-linear properties have to be evaluated inversely each. Thus, depending on a required torque
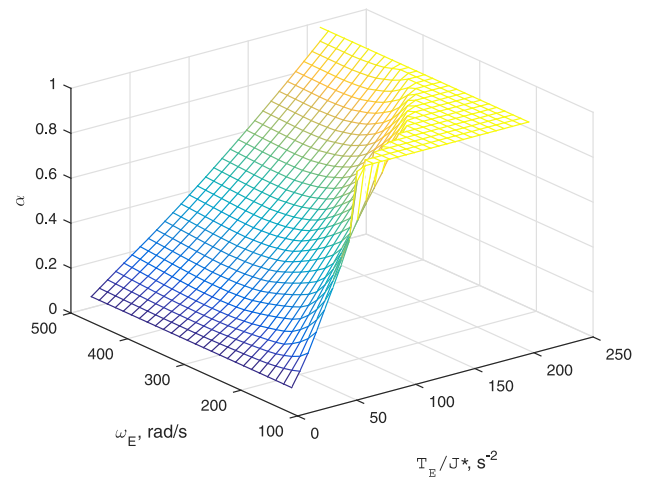

Fig. 12. Inverted engine characteristic.

value, the required pedal positions have to be found. As the clutch torque transmissibility (Fig. 11) is a bijective function (except for $T_{Cl} = 0$ where any arbitrary clutch pedal position above the engagement point can be used) its inverse application is straightforward.

The engine torque characteristic (see Eq. (22) and Fig. 7) depends on the position α and on the engine speed ω_E. With the current engine speed being known, the inversion of the characteristic is achieved numerically. Again, for common internal combustion engines a bijective mapping is obtained. Regions of infeasible torque demand, which appear due to the maximum torque depending on the engine speed, are covered with the extrema of α in the inversion. Fig. 12 depicts the inverted engine characteristic.

4. Feedback linearising control of multivariable systems

By feedback linearisation a system transformation of a non-linear system into equivalent linear systems through a change of variables and suitable control inputs is performed such that it renders a decoupled linear input–output map between new (virtual) inputs and the outputs [1,44,45]. When multivariable systems [46,47] are considered, especially the decoupling property achieved by feedback linearisation is an essential benefit.

4.1. Basic concept

Consider the square non-linear state space system

$$\dot{\boldsymbol{x}} = \boldsymbol{f}(\boldsymbol{x}) + \sum_{i=1}^{m} \boldsymbol{g}_i(\boldsymbol{x})\, u_i \tag{24a}$$

$$y_j = h_j(\boldsymbol{x}), \quad j = 1, \ldots, m \tag{24b}$$

with state vector $\boldsymbol{x} \in \mathbb{R}^{n \times 1}$, scalar inputs u_i, $i = 1, \ldots, m$, scalar outputs y_j, $j = 1, \ldots, m$, smooth vector fields $\boldsymbol{f}(\boldsymbol{x}) : \mathbb{R}^{n \times 1} \rightarrow \mathbb{R}^{n \times 1}$ and $\boldsymbol{g}_i(\boldsymbol{x}) : \mathbb{R}^{n \times 1} \rightarrow \mathbb{R}^{n \times 1}$ as well as smooth output functions $h_j(\boldsymbol{x}) : \mathbb{R}^{n \times 1} \rightarrow \mathbb{R}$. Feedback linearising control is based on differential geometric properties of (24). Thus, time derivatives of the outputs y_j are considered. The first derivative of y_j yields

$$\dot{y}_j = \frac{\partial h_j(\boldsymbol{x})}{\partial \boldsymbol{x}} \frac{\mathrm{d}\boldsymbol{x}}{\mathrm{d}t} = \frac{\partial h_j(\boldsymbol{x})}{\partial \boldsymbol{x}} \left(\boldsymbol{f}(\boldsymbol{x}) + \sum_{i=1}^{m} \boldsymbol{g}_i(\boldsymbol{x})\, u_i \right) \tag{25a}$$

$$= \mathrm{L}_{\boldsymbol{f}} h_j(\boldsymbol{x}) + \sum_{i=1}^{m} \mathrm{L}_{\boldsymbol{g}_i} h_j(\boldsymbol{x})\, u_i. \tag{25b}$$

The expressions $L_f h_j(\boldsymbol{x}) \in \mathbb{R}$ and $L_{\boldsymbol{g}_i} h_j(\boldsymbol{x}) \in \mathbb{R}$ in (25b) are the Lie derivatives [45] of the scalar function $h_j(\boldsymbol{x})$ along the vector fields $\boldsymbol{f}(\boldsymbol{x})$ and $\boldsymbol{g}_i(\boldsymbol{x})$, respectively. The Lie derivative $L_{\boldsymbol{f}}^k h_j(\boldsymbol{x})$, $k \in \mathbb{N}$ is defined recursively

$$L_{\boldsymbol{f}}^k h_j(\boldsymbol{x}) = L_{\boldsymbol{f}}\left(L_{\boldsymbol{f}}^{k-1} h_j(\boldsymbol{x})\right), \tag{26a}$$

$$L_{\boldsymbol{f}}^0 h_j(\boldsymbol{x}) = h_j(\boldsymbol{x}). \tag{26b}$$

The relative degree δ_j of output y_j of system (24) is defined as the number of differentiations which have to be applied before any of the inputs appears in the differentiation for the first time explicitly. Thus, by using Lie derivatives, δ_j is determined from

$$L_{\boldsymbol{g}_i} L_{\boldsymbol{f}}^k h_j(\boldsymbol{x}) = 0, \quad k = 0, \dots, \delta_j - 2, \quad \forall\, i \tag{27a}$$

$$L_{\boldsymbol{g}_i} L_{\boldsymbol{f}}^{\delta_j - 1} h_j(\boldsymbol{x}) \neq 0. \tag{27b}$$

The overall system (24) is said to have relative degree $\Delta = \sum_{j=0}^m \delta_j$ and vector relative degree $[\delta_1, \delta_2, \dots, \delta_m]$. Applying δ_j differentiations to the output y_j yields

$$y_j^{(\delta_j)} = L_{\boldsymbol{f}}^{\delta_j} h_j(\boldsymbol{x}) + \sum_{i=1}^m L_{\boldsymbol{g}_i} L_{\boldsymbol{f}}^{\delta_j - 1} h_j(\boldsymbol{x})\, u_i, \tag{28}$$

which can be written as

$$\begin{bmatrix} y_1^{(\delta_1)} \\ \vdots \\ y_{m-1}^{(\delta_{m-1})} \\ y_m^{(\delta_m)} \end{bmatrix} = \underbrace{\begin{bmatrix} L_{\boldsymbol{f}}^{\delta_1} h_1(\boldsymbol{x}) \\ \vdots \\ L_{\boldsymbol{f}}^{\delta_{m-1}} h_{m-1}(\boldsymbol{x}) \\ L_{\boldsymbol{f}}^{\delta_m} h_m(\boldsymbol{x}) \end{bmatrix}}_{\boldsymbol{l}(\boldsymbol{x})} + \boldsymbol{J}(\boldsymbol{x}) \underbrace{\begin{bmatrix} u_1 \\ \vdots \\ u_{m-1} \\ u_m \end{bmatrix}}_{\boldsymbol{u}} \tag{29}$$

for all m outputs of (24). The matrix $\boldsymbol{J}(\boldsymbol{x}) \in \mathbb{R}^{m \times m}$

$$\boldsymbol{J}(\boldsymbol{x}) = \begin{bmatrix} L_{\boldsymbol{g}_1} L_{\boldsymbol{f}}^{\delta_1 - 1} h_1(\boldsymbol{x}) & \cdots & L_{\boldsymbol{g}_m} L_{\boldsymbol{f}}^{\delta_1 - 1} h_1(\boldsymbol{x}) \\ L_{\boldsymbol{g}_1} L_{\boldsymbol{f}}^{\delta_2 - 1} h_2(\boldsymbol{x}) & \cdots & L_{\boldsymbol{g}_m} L_{\boldsymbol{f}}^{\delta_2 - 1} h_2(\boldsymbol{x}) \\ \vdots & \ddots & \vdots \\ L_{\boldsymbol{g}_1} L_{\boldsymbol{f}}^{\delta_m - 1} h_m(\boldsymbol{x}) & \cdots & L_{\boldsymbol{g}_m} L_{\boldsymbol{f}}^{\delta_m - 1} h_m(\boldsymbol{x}) \end{bmatrix} \tag{30}$$

is the decoupling matrix, which is required to be regular for control. By choosing the control law as

$$\boldsymbol{u} = \boldsymbol{J}^{-1}(\boldsymbol{x})\left(\boldsymbol{v} - \boldsymbol{l}(\boldsymbol{x})\right), \tag{31}$$

an exactly linear and decoupled input–output behaviour from the new virtual input $\boldsymbol{v} \in \mathbb{R}^{m \times 1}$ to the output $\boldsymbol{y}$ in form of integrator chains

$$\begin{bmatrix} y_1^{(\delta_1)} \\ \vdots \\ y_{m-1}^{(\delta_{m-1})} \\ y_m^{(\delta_m)} \end{bmatrix} = \begin{bmatrix} v_1 \\ \vdots \\ v_{m-1} \\ v_m \end{bmatrix} \tag{32}$$

of length δ_j, $j = 1, \dots, m$ is obtained. For systems with full relative degree $\Delta = \sum_{j=1}^m \delta_j = \dim(\boldsymbol{x}) = n$, the state transformation $\Phi(\boldsymbol{x}) : \mathbb{R}^{n \times 1} \to \mathbb{R}^{n \times 1}$

$$\boldsymbol{z} = \begin{bmatrix} z_1 \\ z_2 \\ \vdots \\ z_{\delta_1} \\ z_{\delta_1 + 1} \\ \vdots \\ z_n \end{bmatrix} = \Phi(\boldsymbol{x}) = \begin{bmatrix} h_1(\boldsymbol{x}) \\ L_{\boldsymbol{f}} h_1(\boldsymbol{x}) \\ \vdots \\ L_{\boldsymbol{f}}^{\delta_1 - 1} h_1(\boldsymbol{x}) \\ h_2(\boldsymbol{x}) \\ \vdots \\ L_{\boldsymbol{f}}^{\delta_m - 1} h_m(\boldsymbol{x}) \end{bmatrix} \tag{33}$$
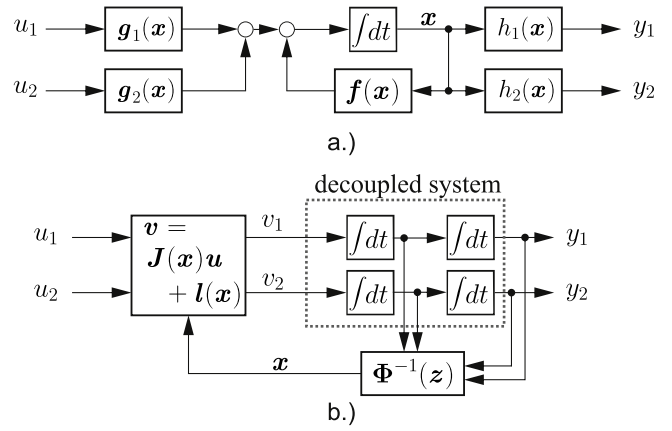

Fig. 13. (a) Original system representation (24); (b) transformed system representation with decoupled dynamics from the virtual inputs v to the outputs y.

in combination with the input transformation

$$\boldsymbol{v} = \boldsymbol{J}(\boldsymbol{x})\boldsymbol{u} + \boldsymbol{l}(\boldsymbol{x}) \tag{34}$$

transforms the original system (24) into its Brunovsky canonical form [1]

$$\dot{\boldsymbol{z}} = \underbrace{\begin{bmatrix} \boldsymbol{A}_{11} & \boldsymbol{0} & \cdots & \boldsymbol{0} \\ \boldsymbol{0} & \boldsymbol{A}_{22} & \cdots & \boldsymbol{0} \\ \vdots & \vdots & \ddots & \vdots \\ \boldsymbol{0} & \boldsymbol{0} & \cdots & \boldsymbol{A}_{mm} \end{bmatrix}}_{\bar{\boldsymbol{A}}} \boldsymbol{z} + \underbrace{\begin{bmatrix} \boldsymbol{b}_{11} & \boldsymbol{0} & \cdots & \boldsymbol{0} \\ \boldsymbol{0} & \boldsymbol{b}_{22} & \cdots & \boldsymbol{0} \\ \vdots & \vdots & \ddots & \vdots \\ \boldsymbol{0} & \boldsymbol{0} & \cdots & \boldsymbol{b}_{mm} \end{bmatrix}}_{\bar{\boldsymbol{B}}} \begin{bmatrix} v_1 \\ v_2 \\ \vdots \\ v_m \end{bmatrix} \tag{35}$$

where $\bar{\boldsymbol{A}} \in \mathbb{R}^{n \times n}$ and $\bar{\boldsymbol{B}} \in \mathbb{R}^{n \times m}$. The m decoupled subsystems of (35) described by matrices $\boldsymbol{A}_{jj} \in \mathbb{R}^{\delta_j \times \delta_j}$

$$\boldsymbol{A}_{jj} = \begin{bmatrix} 0 & 1 & 0 & \cdots & 0 \\ 0 & 0 & 1 & \cdots & 0 \\ \vdots & \vdots & \vdots & \ddots & \vdots \\ 0 & 0 & 0 & \cdots & 1 \\ 0 & 0 & 0 & \cdots & 0 \end{bmatrix} \tag{36}$$

and $\boldsymbol{b}_{jj} \in \mathbb{R}^{\delta_j \times 1}$

$$\boldsymbol{b}_{jj} = \begin{bmatrix} 0 & 0 & \cdots & 0 & 1 \end{bmatrix}^{\mathrm{T}} \tag{37}$$

represent one integrator chain of (32) each. To obtain a non-linear decoupling control law for the original system (24), m linear controllers are designed for each subsystem control signal v_j individually. Finally, the resulting vector $\boldsymbol{v}$ is transformed non-linearly to the physical control signals $\boldsymbol{u}$ by (31). The controller design as well as the resulting control law will be demonstrated in detail for the driveaway control in Section 4.2.

In Fig. 13 a block diagram representation of the original system (24) in subfigure (a) and the transformed system with equivalent input–output behaviour in subfigure (b) are shown. In these block diagrams $m = 2$ and $\delta_1 = \delta_2 = 2$ has been used.

If system (24) does not have full relative degree (i. e. $\Delta < n$), the state transformation $\Phi(\boldsymbol{x})$ is not completely defined by (33). Additional states, which constitute the so called internal dynamics, have to be introduced. For the further treatment of such systems in control, reference may be given to [1] or [45]. In the literature numerous applications of multivariate feedback linearising decoupling control exist, such as for example to vehicle dynamic control [48], to gas conditioning systems [49] or to power systems [50].

4.2. Decoupling launch control

To separate the dynamic properties of the torque buildup models of the engine and the clutch from its static non-linearities, the control loop is based on torques as manipulated variables. The demand values determined by the controller are then inversely transformed to the pedal positions by using the static non-linearity.

The dynamic model used in control incorporates the state vector $\boldsymbol{x} \in \mathbb{R}^{4\times 1}$

$$\boldsymbol{x} = [\omega_{\mathrm{E}},\ \omega_{\mathrm{Cl}},\ T_{\mathrm{E}},\ T_{\mathrm{Cl}}]^{\mathrm{T}} \tag{38}$$

containing the rotational speeds of the engine ω_{E} and the clutch disc ω_{Cl}, as well as the engine and clutch torques T_{E} and T_{Cl}. Their dynamical relations are given by (1), (9) and the dynamic parts of the Wiener models in form of (14). The two outputs are the engine speed and the vehicle speed

$$\boldsymbol{y} = \boldsymbol{h}(\boldsymbol{x}) = \left[x_1,\ \frac{R_{\mathrm{W}}}{r_i}x_2\right]^{\mathrm{T}}, \tag{39}$$

and the manipulated variables are the required torques $T_{\mathrm{E,dmd}}$ and $T_{\mathrm{Cl,dmd}}$

$$\boldsymbol{u} = \left[T_{\mathrm{E,dmd}},\ T_{\mathrm{Cl,dmd}}\right]^{\mathrm{T}}. \tag{40}$$

Giving (24a) in matrix notation with the input matrix $\boldsymbol{G}(\boldsymbol{x}) \in \mathbb{R}^{4\times 2}$ yields

$$\dot{\boldsymbol{x}} = \boldsymbol{f}(\boldsymbol{x}) + \boldsymbol{G}(\boldsymbol{x})\boldsymbol{u}. \tag{41}$$

In the sequel, the derivation of the control law is shown using general formulations of the dynamic parts of the torque models

$$\boldsymbol{G}(\boldsymbol{x}) = [\boldsymbol{g}_1(\boldsymbol{x}),\ \boldsymbol{g}_2(\boldsymbol{x})] = \begin{bmatrix} 0 & 0 \\ 0 & 0 \\ g_{\mathrm{E}}(\boldsymbol{x}) & 0 \\ 0 & g_{\mathrm{Cl}}(\boldsymbol{x}) \end{bmatrix} \tag{42}$$

$$\boldsymbol{f}(\boldsymbol{x}) = \begin{bmatrix} \frac{1}{J_{\mathrm{E}}}(x_3 - x_4) \\ \frac{1}{J'_{\mathrm{V},i}}(x_4 - T'_{\mathrm{R},i}(x_2)) \\ f_{\mathrm{E}}(\boldsymbol{x}) \\ f_{\mathrm{Cl}}(\boldsymbol{x}) \end{bmatrix}. \tag{43}$$

Assessing the relative degrees of the outputs of this system according to (27), reveals that $\delta_1 = 2$, $\delta_2 = 2$ and $\Delta = 4$ holds, which means a system with full relative degree is present.

The decoupling matrix $\boldsymbol{J}(\boldsymbol{x})$ with $m = 2$ is evaluated for the dynamical system (41) consisting of (39), (40), (42) and (43)

$$\boldsymbol{J}(\boldsymbol{x}) = \begin{bmatrix} \frac{1}{J_{\mathrm{E}}}g_{\mathrm{E}}(\boldsymbol{x}) & -\frac{1}{J_{\mathrm{E}}}g_{\mathrm{Cl}}(\boldsymbol{x}) \\ 0 & \frac{R_{\mathrm{W}}}{r_i J'_{\mathrm{V},i}}g_{\mathrm{Cl}}(\boldsymbol{x}) \end{bmatrix}. \tag{44}$$

To complete the input transformation (34), the second order Lie derivatives are required to obtain

$$\boldsymbol{l}(\boldsymbol{x}) = \begin{bmatrix} \frac{1}{J_{\mathrm{E}}}\left(f_{\mathrm{E}}(\boldsymbol{x}) - f_{\mathrm{Cl}}(\boldsymbol{x})\right) \\ \frac{R_{\mathrm{W}}}{r_i J'_{\mathrm{V},i}}\left(f_{\mathrm{Cl}}(\boldsymbol{x}) - \frac{\partial T'_{\mathrm{R},i}(x_2)}{\partial x_2}\left(\frac{x_4}{J'_{\mathrm{V},i}} - \frac{T'_{\mathrm{R},i}(x_2)}{J'_{\mathrm{V},i}}\right)\right) \end{bmatrix}. \tag{45}$$

The state transformation

$$\boldsymbol{z} = \Phi(\boldsymbol{x}) = \begin{bmatrix} x_1 \\ \frac{1}{J_{\mathrm{E}}}(x_3 - x_4) \\ \frac{R_{\mathrm{W}}}{r_i}x_2 \\ \frac{R_{\mathrm{W}}}{r_i J'_{\mathrm{V},i}}\left(x_4 - T'_{\mathrm{R},i}(x_2)\right) \end{bmatrix} \tag{46}$$

and inverse transformation

$$\boldsymbol{x} = \Phi^{-1}(\boldsymbol{z}) = \begin{bmatrix} z_1 \\ \frac{r_i}{R_{\mathrm{W}}}z_3 \\ T'_{\mathrm{R},i}\left(\frac{r_i}{R_{\mathrm{W}}}z_3\right) + \frac{r_i J'_{\mathrm{V},i}}{R_{\mathrm{W}}}z_4 + J_{\mathrm{E}}z_2 \\ T'_{\mathrm{R},i}\left(\frac{r_i}{R_{\mathrm{W}}}z_3\right) + \frac{r_i J'_{\mathrm{V},i}}{R_{\mathrm{W}}}z_4 \end{bmatrix} \tag{47}$$

allow to represent the system in Brunovsky canonical form (35). A linear controller is applied then to each subsystem of (35) described by (36) and (37) to obtain the virtual control signals v_1 and v_2. The physically manipulated variable $\boldsymbol{u}$ follows from the combination of the control law for $\boldsymbol{v}$, (31) and (47).

When the dynamic part of the torque characteristic is a first order low pass, where the time constant τ_{E} may also be a function of engine speed, the following relations hold

$$g_{\mathrm{E}}(\boldsymbol{x}) = \tau_{\mathrm{E}}(x_1)^{-1} \tag{48}$$

$$g_{\mathrm{Cl}}(\boldsymbol{x}) = \tau_{\mathrm{Cl}}^{-1} = g_{\mathrm{Cl}} \tag{49}$$

$$f_{\mathrm{E}}(\boldsymbol{x}) = -\tau_{\mathrm{E}}^{-1}x_3 \tag{50}$$

$$f_{\mathrm{Cl}}(\boldsymbol{x}) = -\tau_{\mathrm{Cl}}^{-1}x_4. \tag{51}$$

As a consequence, the decoupling matrix (30) can be written as

$$\boldsymbol{J}(\boldsymbol{x}) = \begin{bmatrix} (J_{\mathrm{E}}\tau_{\mathrm{E}}(x_1))^{-1} & -(J_{\mathrm{E}}\tau_{\mathrm{Cl}})^{-1} \\ 0 & \frac{R_{\mathrm{W}}}{r_i J'_{\mathrm{V},i}\tau_{\mathrm{Cl}}} \end{bmatrix} \tag{52}$$

and the term $\boldsymbol{l}(\boldsymbol{x})$ reads as

$$\boldsymbol{l}(\boldsymbol{x}) = \begin{bmatrix} J_{\mathrm{E}}^{-1}\left(\tau_{\mathrm{Cl}}^{-1}x_4 - \tau_{\mathrm{E}}^{-1}x_3\right) \\ -\frac{R_{\mathrm{W}}}{r_i J'_{\mathrm{V},i}}\left(\tau_{\mathrm{Cl}}^{-1}x_4 + \frac{1}{J'_{\mathrm{V},i}}\frac{\partial T'_{\mathrm{R},i}(x_2)}{\partial x_2}\left(x_4 - T'_{\mathrm{R},i}(x_2)\right)\right) \end{bmatrix}. \tag{53}$$

The derivative $\frac{\partial T'_{\mathrm{R},i}(x_2)}{\partial x_2}$ is found from (19), where the acceleration a_{Cd} is expressed in form of its polynomial approximation (12), which can be derived analytically with respect to x_2.

4.3. Robustness

To assess the robustness of the decoupling control with respect to parameter uncertainties resulting from identification, a lemma from non-linear control theory is applied. For a simplified notation, the input transformation (31) is rewritten as

$$\boldsymbol{u} = \boldsymbol{\mu}(\boldsymbol{x}) + \boldsymbol{\psi}(\boldsymbol{x})\boldsymbol{v} \tag{54}$$

using abbreviations $\boldsymbol{\psi} \in \mathbb{R}^{m\times m}$ and $\boldsymbol{\mu} \in \mathbb{R}^{m\times 1}$. Their dependencies on $\boldsymbol{x}$ are not further indicated in the sequel. To obtain the error dynamics of the considered system the vector of control errors $\boldsymbol{e} \in \mathbb{R}^{n\times 1}$ is introduced:

$$\boldsymbol{e} = \begin{bmatrix} z_1 - w_1 \\ z_2 - \dot{w}_1 \\ \vdots \\ z_n - w_m^{(\delta_m - 1)} \end{bmatrix}, \tag{55}$$

where w_j indicates the reference trajectory of output j. By a change of coordinates, the Brunovsky canonical form (35) transforms into the error dynamics

$$\dot{\boldsymbol{e}} = \overline{\boldsymbol{A}}\boldsymbol{e} + \overline{\boldsymbol{B}}\left(\boldsymbol{v} - \boldsymbol{w}^{(\delta)}\right). \tag{56}$$

The vector $\boldsymbol{w}^{(\delta)} \in \mathbb{R}^{m\times 1}$ contains the highest derivatives of the reference trajectories

$$\boldsymbol{w}^{(\delta)} = \left[w_1^{(\delta_1)},\ \cdots,\ w_m^{(\delta_m)}\right]^{\mathrm{T}}. \tag{57}$$
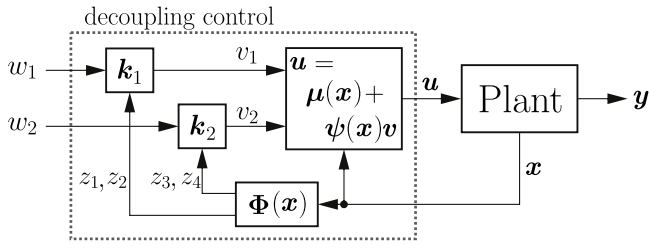
Fig. 14. Closed loop scheme of the decoupling controller for a multivariate system with $m = 2$, $n = 4$ and full relative degree.

Applying state vector feedback $v = -Ke$ with the gain matrix $K \in \mathbb{R}^{m \times n}$ defined as

$$K = \mathrm{diag}\left(k_1, \cdots, k_m\right) \tag{58}$$

and $k_i \in \mathbb{R}^{1 \times \delta_i}$ as the gain vectors of the individual subsystems, a closed loop formulation of the error dynamics can be obtained. Note that the control errors associated with different outputs do not interact and the closed-loop dynamics of the individual error can be chosen independently of the others. A closed-loop scheme of the decoupling control is given in Fig. 14.

Due to unknown parameter deviations resulting from identification, in the application of the control law it is assumed that only approximations $\hat{\psi}$, $\hat{\mu}$ and $\hat{z} = \hat{\Phi}(x)$ of the actual non-linearities ψ, μ and Φ are known. Finally, the closed loop error dynamics

$$\dot{e} = \left(\overline{A} - \overline{B}K\right)e + \overline{B}\lambda \tag{59}$$

comprise the nominal dynamics and an additional term $\lambda \in \mathbb{R}^{m \times 1}$ acting as perturbation input

$$\lambda = \psi^{-1}\left[\left(\psi - \hat{\psi}\right)\left(Ke - w^{(\delta)}\right) + \hat{\psi}K\left(\Phi - \hat{\Phi}\right) + \hat{\mu} - \mu\right]. \tag{60}$$

All quantities in (60) except the gain matrix K depend on x. To assess the behaviour of the closed-loop system (59), the following lemma [44] is applied:

Lemma 1. *Consider the closed-loop system* (59), *where* $\left(\overline{A} - \overline{B}K\right)$ *is Hurwitz. Let* $P = P^{\mathrm{T}} \succ 0$ *be the solution of the Lyapunov equation*

$$P\left(\overline{A} - \overline{B}K\right) + \left(\overline{A} - \overline{B}K\right)^{\mathrm{T}}P = -I \tag{61}$$

and k be a nonnegative constant less than $\left(2\|P\overline{B}\|_2\right)^{-1}$.

- *If* $\|\lambda\| \leq k\|e\|$ *for all* e, *the origin of* (59) *will be globally exponentially stable.*
- *If* $\|\lambda\| \leq k\|e\| + \epsilon$ *for all* e, *the state* e *will be globally ultimately bounded by* ϵc *for some* $c > 0$.

Simulation results for perturbed parameters of the startup controller will be shown in Section 5.2.

4.4. Control with integral action

To reduce steady-state errors and improve the overall closed-loop behaviour, integration of the control error should be beneficially applied. Thus, the error vector (55) is enhanced by one integrator for each output error such that an additional state e_i^+ is included into e just before state e_i. The dynamics of e_i^+ and the index i are defined as

$$\dot{e}_i^+ = e_i, \quad i = 1, \delta_1 + 1, \dots, \sum_{j=1}^{m-1} \delta_j + 1. \tag{62}$$

The structure of the resulting dynamics of the enhanced error vector $e^+ \in \mathbb{R}^{(n+m) \times 1}$ remains the same as in (56) with the matrix
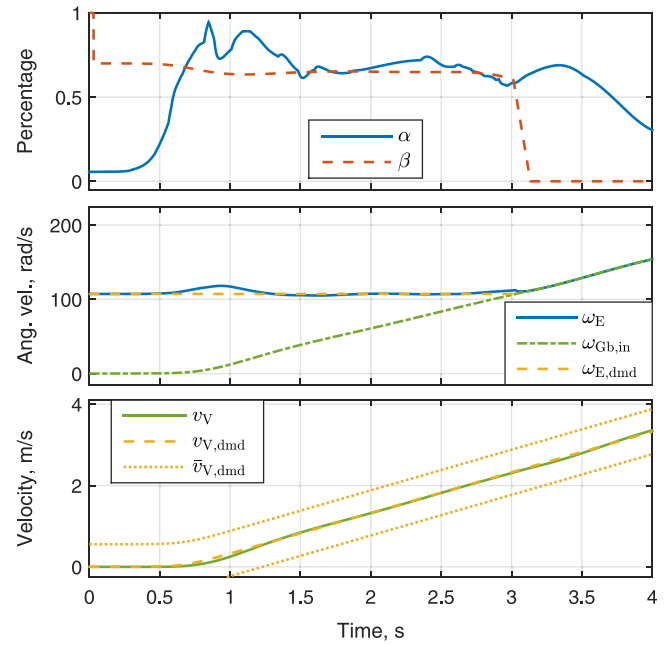

Fig. 15. Simulation result of vehicle launch; Upper panel: accelerator (blue solid line) and clutch pedal position (red dashed line); Middle panel: engine speed (blue solid line), reference trajectory (yellow dashed line) and clutch disc speed (green dash-dotted line); Lower panel: vehicle velocity (green solid line) and reference trajectory (yellow dashed line) as well as the $\pm 2 \, \frac{km}{h}$ tolerance bounds.

Table 1
Vehicle parameters.

m_V	1500 kg	R_W	29.3 cm
J_E	0.07 kg^2	r_1	13.382
$J_{V,1}'$	0.74 kg^2	τE	0.2 s
J^*	$\simeq$0.81 kg^2	τCl	10 ms

dimensions increased accordingly. The application of state vector feedback $v = -K^+e^+$ leads to the same conclusions as drawn without the additional integrator. In the context of feedback linearisation this control approach is also referred to as extended PID or PID$^{\delta-1}$ control [51].

5. Results

To evaluate the proposed control scheme, the multi-disciplinary vehicle simulation software *AVL CRUISE*$^{\mathrm{TM}}$*M* and *IPG CarMaker*® *pro* has been used, whereupon the results of the latter one are depicted in the sequel.

5.1. Nominal results

For simulation a medium-class passenger car with front-wheel drive is used. As the startup performance of the decoupling control has to be assessed, all simulations have been performed in first gear. Relevant vehicle parameters are given in Table 1.

In Fig. 15 the simulation result of a vehicle launch using nominal parameters in the controller are shown. The decoupled feedback controllers have been designed to possess dominant pole couples at $-12.35 \pm 4.06i$ for the engine speed and at $-10.45 \pm 3.43i$ for the vehicle velocity. In addition to the favourable behaviour of the controlled variables as compared to their reference trajectories, also the trajectories of the manipulated variables are beneficial. They do not show any sharp spikes, which would deteriorate the performance related to emission cycle testing. As soon as the slip speed decreased to nearly zero, the clutch is closed
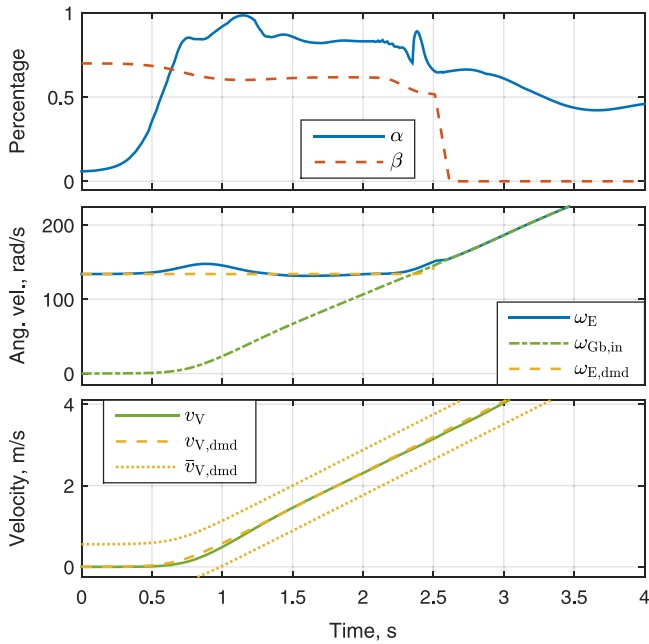
Fig. 16. Simulation result of vehicle launch with increased acceleration (for a detailed description of the panels refer to Fig. 15).

and an alternative one-degree-of-freedom control is applied for velocity tracking (i. e. at shortly after $t = 3$ s in Fig. 15).

In Fig. 16 the simulation is repeated with a different reference trajectory leading to a higher acceleration than in Fig. 15 (1.75 $\frac{m}{s^2}$ instead of 1 $\frac{m}{s^2}$). These acceleration values are comparable or even higher than they appear for example in standardised exhaust-gas test cycles. Also with the higher acceleration reference, the control performance is advantageous.

5.2. Robustness

To assess robustness in the sense of Lemma 1, several parameters in the controller are perturbed considerably and the effect is analysed. The time constant τ_E is set to 140% of its nominal value, inertia J_E to 140%, inertia $J'_{V,1}$ as well as inertia J^* to 85%. These perturbations represent a more inert engine in combination with a more agile powertrain. Evaluating the Lyapunov equation (61) for the applied controller design yields an upper bound of constant k of 5.538. In Fig. 17 the inequality of Lemma 1 incorporating the control error e^+ and perturbation input λ according to (60) is depicted in the time interval the decoupling control is activated. The value of k is set to its upper bound value. If $\|\lambda\| - k\|e^+\|$ remained less or equal to zero, the error dynamics (59) would be globally exponentially stable. In this example, the result in Fig. 17 using the described parameter variation indicates the error dynamics to be bounded. The same result holds for different combinations of physically plausible parameter variations.

In Fig. 18 the simulation of Fig. 15 is repeated with a worn out clutch. Compared to its identified characteristic (Fig. 11), the static relation between torque and clutch pedal position is shifted horizontally by a value of 0.05. This represents an increase in clutch wear. Although the closed-loop performance is decreased slightly, the controller handles the altered characteristic well.

As the drive away control scheme is intended to be used at the beginning of a drive cycle only, a constant clutch temperature is assumed. The consideration of temperature effects would be necessary when frequent high acceleration launches were to be performed. As the robustness against parameter deviations is good, slight influences of temperature can be handled by the controller already.
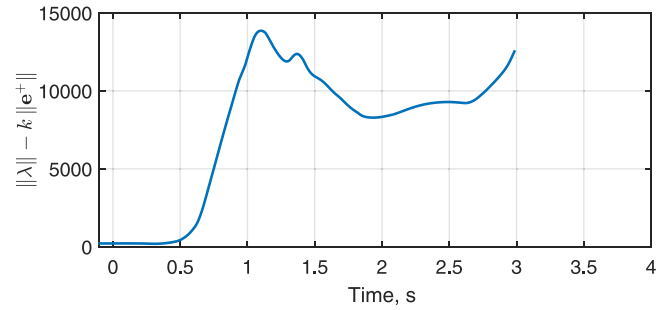

Fig. 17. Assessment of Lemma 1 to show the boundedness of the error dynamics for a variation of model parameters in the controller.
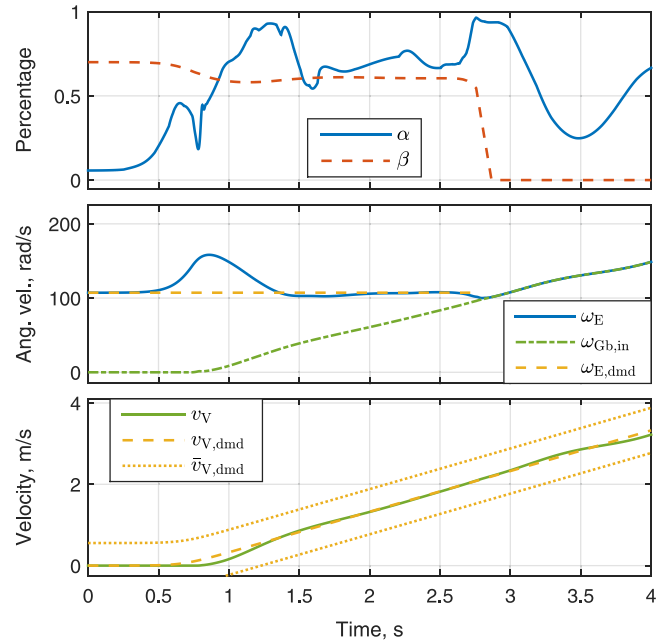

Fig. 18. Simulation result of vehicle launch with additional clutch wear as compared to the identified characteristics (for a detailed description of the panels refer to Fig. 15).

6. Conclusion & outlook

In this paper a holistic workflow to efficiently automate drive-away manoeuvres on a chassis dynamometer testbed without having to spend too much expensive testbed time for vehicle modelling has been described. A suitable powertrain model structure has been combined with an identification procedure, which results in a non-linear vehicle model directly applicable in non-linear multivariate decoupling control using the accelerator and clutch pedal positions as manipulated variables. Therefore, an efficient identification of necessary vehicle characteristics has been applied in combination with a simple design of experiment. The proposed control has been derived using feedback linearisation and significantly facilitates the robust and fully automated chassis dynamometer operation of vehicles with manual transmissions. In the literature, which is reviewed in Section 1, such an procedure focused on efficiency and robustness as well as the proposed control concept has not been covered yet.

Besides the execution of experiments on an actual testbed, as an outlook the decoupling control approach could be extended to non-linear powertrain control for oscillation avoidance. In powertrain testbeds, torques are applied by electric dynamometers directly to the drive shafts. Thus, not the pedal positions but the

dynamometer torques act as manipulated variables. This setup gives the opportunity to eliminate higher frequency oscillations using more complex powertrain models in decoupling control.

Note that the decoupling control scheme is not restricted to the presented model structure or application case. It could be applied with different model structures such as neural networks (e. g. resulting from deep learning) as well. The application of feedback linearisation for decoupling control is possible as long as one is able to deduce the appropriate Lie derivatives.

Declaration of competing interest

The authors declare that they have no known competing financial interests or personal relationships that could have appeared to influence the work reported in this paper.

Acknowledgements

References

[1] Isidori A. Nonlinear control systems. Communications and control engineering, 3rd ed. London: Springer-Verlag; 1995.

[2] Sailer S, Buchholz M, Dietmayer K. Flatness based velocity tracking control of a vehicle on a roller dynamometer using a robotic driver. In: Proceedings of the 50th IEEE conference on decision and control and european control conference. Orlando, USA; 2011. p. 7962–67.

[3] Nelles O. Nonlinear system identification, vol. 13. Measurement science and technology, Springer Berlin Heidelberg; 2001.

[4] Slicker JM, Loh R. Design of robust vehicle launch control system. IEEE Trans Control Syst Technol 1996;4(4):326–35.

[5] Garofalo F, Glielmo L, Iannelli L, Vasca F. smooth engagement for automotive dry clutch. In: Proceedings of the 40th IEEE conference on decision and control. Orlando, USA; 2001. p. 529–34.

[6] Garofalo F, Glielmo L, Iannelli L, Vasca F. Optimal tracking for automotive dry clutch engagement. In: Proceedings of the 15th IFAC world congress. Barcelona, Spain; 2002. p. 367–72.

[7] Serrarens A, Dassen M, Steinbuch M. Simulation and control of an automotive dry clutch. In: Proceedings of the American control conference, vol. 5. Boston, USA; 2004. p. 4078–83.

[8] Dolcini PJ, Canudas de Wit C, Béchart H. Dry clutch control for automotive applications. Advances in industrial control, Springer-Verlag London Limited; 2010.

[9] Gao B, Chen H, Ma Y, Sanada K. Clutch slip control of automatic transmission using nonlinear method. In: Proceedings of the joint 48th IEEE conference on decision and control and 28th Chinese control conference. Shanghai, P.R. China; 2009. p. 7651–56.

[10] Walker PD, Zhang N, Tamba R. Control of gear shifts in dual clutch transmission powertrains. Mech Syst Signal Process 2011;25:1923–36.

[11] van Berkel K, Hofman T, Serrarens A, Steinbuch M. Fast and smooth clutch engagement control for dual-clutch transmissions. Control Eng Pract 2014;22:57–68.

[12] Hu Y, Tian L, Gao B, Chen H. Nonlinear gearshifts control of dual-clutch transmissions during inertia phase. ISA Trans 2014;53(4):1320–31. http://dx.doi.org/10.1016/j.isatra.2014.03.017.

[13] Gao B, Chen H, Hu Y, Sanada K. Nonlinear feedforward–feedback control of clutch-to-clutch shift technique. Veh Syst Dyn 2011;49(12):1895–911. http://dx.doi.org/10.1080/00423114.2011.552617.

[14] Kang M, Shen T. Receding horizon online optimization for torque control of gasoline engines. ISA Trans 2016;65:371–83. http://dx.doi.org/10.1016/j.isatra.2016.06.012.

[15] Gao B, Chen H, Liu Q, Sanada K. Clutch slip control of automatic transmissions: A nonlinear feedforward-feedback design. In: Proceedings of the IEEE international conference on control applications 2010. Yokohama, Japan; 2010. p. 884–9.

[16] Glielmo L, Iannelli L, Vacca V, Vasca F. Gearshift control for automated manual transmissions. IEEE/ASME Trans Mechatronics 2006;11(1):17–26.

[17] David J, Natarajan N. Design of an optimal clutch controller for commercial trucks. In: Proceedings of the American control conference 2005. Portland, USA; 2005. p. 1599–606.

[18] Amari R, Tona P, Alamir M. A phenomenological model for torque transmissibility during dry clutch engagement. In: 18th IEEE international conference on control applications. Saint Petersburg, Russia; 2009. p. 600–6.

[19] Guzzella L, Sciarretta A. Vehicle propulsion systems. 2nd ed. Springer Berlin Heidelberg; 2007.

[20] Guzzella L, Onder C. Introduction to modeling and control of internal combustion engine systems. Springer Berlin Heidelberg; 2009.

[21] Chan CC, Bouscayrol A, Chen K. Electric, hybrid, and fuel-cell vehicles: Architectures and modeling. IEEE Trans Veh Technol 2010;59(2):589–98. http://dx.doi.org/10.1109/TVT.2009.2033605.

[22] Ulsoy AG, Peng H, Cakmakci M. Automotive control systems. Cambridge: Cambridge University Press; 2012.

[23] Mashadi B, Crolla D. Vehicle powertrain systems. West Sussex, UK: John Wiley and Sons; 2012.

[24] Martyr AJ, Plint MA. Engine testing: The design, building, modification and use of powertrain test facilities. Oxford, UK: Elsevier Science; 2012.

[25] Eriksson L, Nielsen L. Modeling and control of engines and drivelines. Automotive series, John Wiley and Sons; 2014.

[26] Barlow TJ, Latham S, McCrae IS, Boulter PG. A reference book of driving cycles for use in the measurement of road vehicle emissions. Published project report PPR354, Wokingham, UK: Transport Research Laboratory Limited; 2009.

[27] Wahlström J, Eriksson L. Modelling diesel engines with a variable-geometry turbocharger and exhaust gas recirculation by optimization of model parameters for capturing non-linear system dynamics. Proc Inst Mech Eng 2011;225(7):960–86.

[28] Togun N, Baysec S, Kara T. Nonlinear modeling and identification of a spark ignition engine torque. Mech Syst Signal Process 2012;26:294–304.

[29] Glielmo L, Iannelli L, Vacca V, Vasca F. Speed control for automated manual transmission with dry clutch. In: 43rd IEEE conference on decision and control; 2004. p. 1709–14.

[30] Deur J, Ivanović V, Herold Z, Kostelac M, Tseng HE. Dry clutch control based on electromechanical actuator position feedback loop. Int J Veh Des 2012;60(3–4):305–26.

[31] Vasca F, Iannelli L, Senatore A, Reale G. Torque transmissibility assessment for automotive dry-clutch engagement. IEEE/ASME Trans Mechatronics 2011;16(3):564–73.

[32] Horn J, Bamberger J, Michau P, Pindl S. Flatness-based clutch control for automated manual transmissions. Control Eng Pract 2003;11:1335–59.

[33] Myklebust A, Eriksson L. Modeling, observability, and estimation of thermal effects and aging on transmitted torque in a heavy duty truck with a dry clutch. IEEE/ASME Trans Mechatronics 2015;20(1):61–72.

[34] Pacejka H. Tire and vehicle dynamics. 3rd ed. Oxford: Butterworth-Heinemann; 2012.

[35] Ivanov V, Savitski D, Augsburg K, Barber P, Knauder B, Zehetner J. Wheel slip control for all-wheel drive electric vehicle with compensation of road disturbances. J Terramech 2015;61:1–10. http://dx.doi.org/10.1016/j.jterra.2015.06.005.

[36] Shyrokau B, Wang D, Savitski D, Hoepping K, Ivanov V. Vehicle motion control with subsystem prioritization. Mechatronics 2015;30:297–315. http://dx.doi.org/10.1016/j.mechatronics.2014.11.004.

[37] Savitski D, Schleinin D, Ivanov V, Augsburg K, Jimenez E, He R, et al. Improvement of traction performance and off-road mobility for a vehicle with four individual electric motors: Driving over icy road. J Terramech 2017;69:33–43. http://dx.doi.org/10.1016/j.jterra.2016.10.005.

[38] Lu Q, Sorniotti A, Gruber P, Theunissen J, Smet JD. H_∞ loop shaping for the torque-vectoring control of electric vehicles: Theoretical design and experimental assessment. Mechatronics 2016;35:32–43. http://dx.doi.org/10.1016/j.mechatronics.2015.12.005.

[39] Novellis LD, Sorniotti A, Gruber P, Orus J, Fortun J-MR, Theunissen J, et al. Direct yaw moment control actuated through electric drivetrains and friction brakes: Theoretical design and experimental assessment. Mechatronics 2015;26:1–15. http://dx.doi.org/10.1016/j.mechatronics.2014.12.003.

[40] Lu Q, Gentile P, Tota A, Sorniotti A, Gruber P, Costamagna F, et al. Enhancing vehicle cornering limit through sideslip and yaw rate control. Mech Syst Signal Process 2016;75:455–72. http://dx.doi.org/10.1016/j.ymssp.2015.11.028.

[41] Novellis LD, Sorniotti A, Gruber P. Driving modes for designing the cornering response of fully electric vehicles with multiple motors. Mech Syst Signal Process 2015;64:1–15. http://dx.doi.org/10.1016/j.ymssp.2015.03.024.

[42] Škrjanc I, Andonovski G, Ledezmaa A, Sipele O, Martínez JAI, Sanchis A. Evolving cloud-based system for the recognition of drivers' actions. Expert Syst Appl 2018;99:231–8.

[43] Andersson S, Söderberg A, Björklund S. Friction models for sliding dry, boundary and mixed lubricated contacts. Tribol Int 2007;40:580–7.

[44] Khalil HK. Nonlinear systems. 3rd ed. Upper Saddle River: Prentice Hall; 2002.

[45] Slotine J-JE, Li W. Applied nonlinear control. Englewood Cliffs: Prentice Hall; 1991.

[46] Škrjanc I, Blažič S, Oblak S, Richalet J. An approach to predictive control of multivariable time-delayed plant : stability and design issues. ISA Trans 2004;43:585–95.

[47] Preglej A, Rehrl J, Schwingshackl D, Steiner I, Horn M, Škrjanc I. Energy-efficient fuzzy model-based multivariable predictive control of a hvac system. Energy Build 2014;82:520–33.

[48] Menhour L, d'Andrea Novel B, Fliess M, Mounier H. Coupled nonlinear vehicle control: Flatness-based setting with algebraic estimation techniques. Control Eng Pract 2014;22:135–46.

[49] Kancsar J, Striednig M, Aldrian D, Trattner A, Klell M, Kuegele C, et al. A novel approach for dynamic gas conditioning for pemfc stack testing. Int J Hydrogen Energy 2017;42:28898–909.

[50] Akhrif O, Okou F-A, Dessaint L-A, Champagne R. Application of a multi-variable feedback linearization scheme for rotor angle stability and voltage regulation of power systems. IEEE Trans Power Syst 1999;14(2):620–8.

[51] Hagenmeyer V, Delaleau E. Exact feedforward linearization based on differential flatness. Internat J Control 2003;76(6):537–56.